Inorg. Chem. **2007**, *46*, 11122–11132

New Insights into the Visible-Light-Induced DNA Cleavage Activity of Dipyridoquinoxaline Complexes of Bivalent 3d-Metal Ions

Mithun Roy, Biswarup Pathak, Ashis K. Patra, Eluvathingal D. Jemmis,*,† Munirathinam Nethaji, and Akhil R. Chakravarty*,‡

Department of Inorganic and Physical Chemistry, Indian Institute of Science, Bangalore 560012, India

Received July 21, 2007

Dipyridoquinoxaline (dpq) complexes of bivalent 3d-metal ions, viz., $[Fe^{II}(dpq)_3](PF_6)_2$ (**1**), $[Co^{II}(dpq)_3](ClO_4)_2$ (**2**), $[Ni^{II}(dpq)_3](ClO_4)_2$ (**3**), $[Cu^{II}(dpq)_2(H_2O)](ClO_4)_2$ (**4**), $[Zn^{II}(dpq)_3](ClO_4)_2$ (**5**), and $[Zn^{II}(dpq)_2(DMF)_2](ClO_4)_2$ (**5a**) (DMF = *N,N*-dimethylformamide), are prepared and their photoinduced DNA cleavage activity studied. Structural characterization for the complexes **1** and **5a** is done by single-crystal X-ray crystallography. All the complexes show efficient binding propensity to calf thymus DNA with a binding constant (*K*) value of $\sim 10^5$ M^{-1}. Complexes **1**, **2**, and **4** show metal-based cyclic voltammetric responses at 1.2, 0.4, and 0.09 V (vs SCE) in DMF 0.1 M $[Bu^n_4N](ClO_4)$ assignable to the respective Fe^{III}/Fe^{II}, Co^{III}/Co^{II}, and Cu^{II}/Cu^{I} couples. The Ni^{II} and Zn^{II} complexes do not show any metal-based redox process. The dpq-based reductions are observed in the potential range of –1.0 to –1.7 V vs SCE. DNA melting and viscosity data indicate the groove-binding nature of the complexes. Control experiments using distamycin-A suggest a minor groove-binding propensity of the complexes. The complexes exhibit photoinduced cleavage of supercoiled pUC19 DNA in UV light of 365 nm. The diamagnetic d^6-Fe^{II} and d^{10}-Zn^{II} complexes are cleavage-inactive on irradiation with visible light. The paramagnetic d^7-Co^{II} and d^9-Cu^{II} complexes exhibit efficient DNA cleavage activity on photoirradiation at their respective d–d band. The paramagnetic d^8-Ni^{II} complex displays only minor DNA cleavage activity on irradiation at its d–d band. The DNA cleavage reactions at visible light under aerobic conditions involve the formation of hydroxyl radical. The Co^{II} complex shows photocleavage of DNA under an argon atmosphere. Theoretical calculations on the complexes suggest a photoredox pathway in preference to a type-2 process forming singlet oxygen for the visible-light-induced DNA cleavage activity of the 3d-metal complexes. The theoretical data also predict that the photoredox pathway is favorable for the $3d^7$-Co^{II} and $3d^9$-Cu^{II} complexes to exhibit DNA cleavage activity, while the analogous $3d^6$-Fe^{II} and $3d^8$-Ni^{II} complexes are energetically unfavorable for the exhibition of such activity under visible light. The Co^{II} and Cu^{II} complexes are better suited for designing and developing new metal-based PDT agents than their cleavage-inactive Fe^{II}, Ni^{II}, and Zn^{II} analogues.

Introduction

The design and development of compounds that show efficient DNA cleavage activity on low-energy visible light irradiation under physiological conditions are of importance in the chemistry of photodynamic therapy (PDT).[1–5] Organic macrocyclic dyes such as porphyrin and phthalocyanin bases are known to cleave DNA under red light, making them suitable for clinical applications in PDT.[6–12] The currently FDA-approved anticancer PDT drug Photofrin is a hemato-

* To whom correspondence should be addressed. E-mail: jemmis@ipc.iisc.ernet.in (E.D.J.), arc@ipc.iisc.ernet.in (A.R.C.). Fax: 91-80-23601552 (E.D.J.), 91-80-23600683 (A.R.C.).

† Correspondence for computational studies.

‡ Correspondence of a general nature.

(1) Bonnet, R. *Chemical Aspects of Photodynamic Therapy*; Gordon & Breach: London, U.K., 2000.

(2) Sternberg, E. D.; Dolphin, D.; Brückner, C. *Tetrahedron* **1998**, *54*, 4151.

(3) Ali, H.; van Lier, J. E. *Chem. Rev.* **1999**, *99*, 2379.

(4) Henderson, B. W.; Busch, T. M.; Vaughan, L. A.; Frawley, N. P.; Babich, D.; Sosa, T. A.; Zollo, J. D.; Dee, A. S.; Cooper, M. T.; Bellnier, D. A.; Greco, W. R.; Oseroff, A. R. *Cancer Res.* **2000**, *60*, 525.

(5) DeRosa, M. C.; Crutchley, R. J. *Coord. Chem. Rev.* **2002**, *233–234*, 351.

(6) Allen, C. M.; Sharman, W. M.; van Lier, J. E. *Tumor Targeting Cancer Ther.* **2002**, 329.

10.1021/ic701450a CCC: $37.00
Published on Web 11/29/2007

porphyrin species that acts on irradiation at its lowest energy Q band with light of 630 nm wavelength.[1] Since this particular drug shows significant skin and hepatotoxicity, there is a surge of research activity to develop a new generation of less toxic PDT drugs.[13−18] Besides such macrocyclic bases, water-soluble non-macrocylic organic dyes such as distyryl-boradiazaindacenes are reported to efficiently cleave DNA in the phototherapeutic window.[19] In addition to the organic dyes, transition-metal complexes have increasingly been used to study the cleavage of double-stranded DNA by photochemical means using visible light.[20−29] While organic dyes used in PDT cleave DNA aerobically by a singlet oxygen pathway in which the long-lived $^3\pi\pi^*$ state of the dye transfers energy to the triplet molecular oxygen ($^3O_2$) to form cytotoxic singlet oxygen species ($^1O_2$) in a type-2 pathway, transition-metal complexes with tunable coordination environments and versatile spectral and electrochemical properties offer a greater scope of design for species that are suitable for the photocleavage of DNA following the singlet oxygen and/or photoredox pathways.[30−32] The DNA photocleavage by ruthenium(II) polypyridyl complexes having intercalating bases generally follows the singlet oxygen (type-2) mechanism.[20] The copper(II) complexes having photoactive phenanthroline bases, however, are known to follow both the singlet oxygen and photoredox pathways.[25,26] An exclusive photoredox pathway for DNA cleavage under visible light is reported for an iron(III) complex.[33]

Metal complexes are known to cleave DNA by oxidative and hydrolytic pathways. Hydrolytic cleavage of DNA takes place due to hydrolysis of the phosphodiester linkage forming fragments that could be subsequently religated.[34−36] Metal ions with strong Lewis acidity show hydrolytic cleavage of DNA, thus modeling restriction enzyme activity. The oxidative cleavage of DNA, on the other hand, leads to the degradation of the DNA molecule to fragments either due to the abstraction of the deoxyribose sugar hydrogen atom(s) or the oxidation of the guanine base.[37−40] Among the nucleobases, guanine, with the lowest oxidation potential, is most susceptible to oxidation.[20] DNA cleavage by the oxidative method is used in footprinting studies and in chemotherapeutic applications. In recent years, there is a growing interest in the design of metal complexes cleaving DNA on photoirradiation for their potential use in PDT because of the noninvasive nature of this therapeutic process requiring photoactivation of the drug at the tumor cells, leaving other healthy cells unexposed to light.[1,20,21] Recent reports by Turro−Dunbar and co-workers have shown that dirhodium(II) compounds with photoactive phenanthroline bases have potentials for medicinal applications in PDT.[29] The rhodium(II) compounds show photonuclease activity via oxygen-dependent and independent pathways with signifi-

(7) Rodriguez, M. E.; Moran, F.; Bonansea, A.; Monetti, M.; Fernandez, D. A.; Strassert, C. A.; Rivarola, V.; Awruch, J.; Dicelio, L. E. *Photochem. Photobiol. Sci.* **2003**, *2*, 988.
(8) Wei, W.-H.; Wang, Z.; Mizuno, T.; Cortez, C.; Fu, L.; Sirisawad, M.; Naumovski, L.; Magda, D.; Sessler, J. L. *Dalton Trans.* **2006**, 1934. Young, S. W.; Woodburn, K. W.; Wright, M.; Mody, T. D.; Fan, Q.; Sessler, J. L.; Dow, W. C.; Miller, R. A. *Photochem. Photobiol.* **1996**, *63*, 892.
(9) Peng, Q.; Warloe, T.; Berg, K.; Moan, J.; Kongshaug, M.; Giercsky, K.-E.; Nesland, J. M. *Cancer* **1997**, *79*, 2282. Kennedy, J. C.; Pottier, R. H.; Pross, D. C. *J. Photochem. Photobiol., B* **1990**, *6*, 143.
(10) Dilkes, M. G.; De Jode, M. L.; Rowntree-Taylor, A. *Lasers Med. Sci.* **1997**, *11*, 23. Bonnett, R.; White, R. D.; Winfield, U.-J.; Berenbaum, M. C. *Biochem. J.* **1989**, *261*, 277. Razum, N.; Snyder, A.; Dorion, D. *Proc. SPIE—Int. Soc. Opt. Eng.* **1996**, *2675*, 43. Morgan, A. R.; Garbo, G. M.; Keck, R. W.; Selman, S. H. *Cancer Res.* **1988**, *48*, 194.
(11) Nelson, J. S.; Roberts, W. G.; Berns, J. W. *Cancer Res.* **1987**, *46*, 4681. Pandey, R. K.; Sumlin, A. B.; Constantine, S.; Aoudia, M.; Potter, W. R.; Bellnier, D. A.; Henderson, B. W.; Rodgers, M. A.; Smith, K. M.; Dougherty, T. J. *Photochem. Photobiol.* **1996**, *64*, 194.
(12) Stranadko, E.; Skobelkin, O.; Litwin, G.; Astrakhankina, T. *Proc. SPIE—Int. Soc. Opt. Eng.* **1994**, *2325*, 240. Richter, A. M.; Kelly, B.; Chow, J.; Liu, D. J.; Towers, G. M. N.; Dolphin, D.; Levy, J. G. *J. Natl. Cancer. Inst.* **1987**, *79*, 1327. Levy, J. G.; Chan, A.; Strong, H. A. *Proc. SPIE—Int. Soc. Opt. Eng.* **1996**, *2625*, 86.
(13) McDonnell, S. O.; Hall, M. J.; Allen, L. T.; Byrne, A.; Gallagher, W. M.; O'Shea, D. F. *J. Am. Chem. Soc.* **2005**, *127*, 16360.
(14) Ramaiah, D.; Eckert, I.; Arun, K. T.; Weidenfeller, L.; Epe, B. *Photochem. Photobiol.* **2004**, *79*, 99.
(15) Li, G.; Pandey, S. K.; Dobhal, M. P.; Mehta, R.; Chen, Y.; Gryshuk, A.; Olson, K.; Oseroff, A. R.; Pandey, R. K. *J. Org. Chem.* **2004**, *69*, 158.
(16) Detty, M. R.; Gibson, S. L.; Wagner, S. J. *J. Med. Chem.* **2004**, *47*, 3897. Yukruk, F.; Dogan, A. L.; Canpinar, H.; Guc, D.; Akkaya, E. U. *Org. Lett.* **2005**, *7*, 2885.
(17) Sessler, J. L.; Miller, R. A. *Biochem. Pharmacol.* **2000**, *59*, 733. Magda, D. J.; Wang, Z.; Gerasimchuk, N.; Wei, W.; Anzenbacher, P.; Sessler, J. L. *Pure Appl. Chem.* **2004**, *76*, 365.
(18) Martina, E. W.; Hone, D. C.; Cook, M. J.; Handsley, M. M.; Gavrilovic, J.; Russell, D. A. *Photochem. Photobiol. Sci.* **2006**, *5*, 727.
(19) Atilgan, S.; Ekmekci, Z.; Dogan, A. L.; Guc, D.; Akkaya, E. U. *Chem. Commun.* **2006**, 4398.
(20) Erkkila, K. E.; Odom, D. T.; Barton, J. K. *Chem. Rev.* **1999**, *99*, 2777.
(21) Chifotides, H. T.; Dunbar, K. R. *Acc. Chem. Res.* **2005**, *38*, 146.
(22) Dobrucki, J. W. *J. Photochem. Photobiol., B* **2001**, *65*, 136. Arounaguiri, S.; Maiya, B. G. *Inorg. Chem.* **1996**, *35*, 4267.
(23) Kraft, B. J.; Zaleski, J. M. *New J. Chem.* **2001**, *25*, 1281.
(24) Holder, A. A.; Swavey, S.; Brewer, K. J. *Inorg. Chem.* **2004**, *43*, 303. Holder, A. A.; Zigler, D. F.; Tarrago-Trani, M.; Storrie, B.; Brewer, K. J. *Inorg. Chem.* **2007**, *46*, 4760.
(25) Dhar, S.; Senapati, D.; Das, P. K.; Chattopadhyay, P.; Nethaji, M.; Chakravarty, A. R. *J. Am. Chem. Soc.* **2003**, *125*, 12118. Dhar, S.; Nethaji, M.; Chakravarty, A. R. *Inorg. Chem.* **2006**, *45*, 11043.
(26) Dhar, S.; Senapati, D.; Reddy, P. A. N.; Das, P. K.; Chakravarty, A. R. *Chem. Commun.* **2003**, 2452.
(27) Meunier, B. *Chem. Rev.* **1992**, *92*, 1411. Reedijk, J. *J. Inorg. Biochem.* **2001**, *86*, 89.
(28) Hergueta-Bravo, A.; Jiménez-Hernández, M. E.; Montero, F.; Oliveros, E.; Orellana, G. *J. Phys. Chem. B* **2002**, *106*, 4010.
(29) Chouai, A.; Wicke, S. E.; Turro, C.; Bacsa, J.; Dunbar, K. R.; Wang, D.; Thummel, R. P. *Inorg. Chem.* **2005**, *44*, 5996. Angeles-Boza, A. M.; Bradley, P. M.; Fu, P. K.-L.; Shatruk, M.; Hilfiger, M. G.; Dunbar, K. R.; Turro, C. *Inorg. Chem.* **2005**, *44*, 7262. Bradley, P. M.; Angeles-Boza, A. M.; Dunbar, K. R.; Turro, C. *Inorg. Chem.* **2004**, *53*, 2450. Angeles-Boza, A. M.; Bradley, P. M.; Fu, P. K.-L.; Wicke, S. E.; Bacsa, J.; Dunbar, K. R.; Turro, C. *Inorg. Chem.* **2004**, *43*, 8510.
(30) Szacilowski, K.; Macyk, W.; Drzewiecka-Matuszek, A.; Brindell, M.; Stochel, G. *Chem. Rev.* **2005**, *105*, 2647. Armitage, B. *Chem. Rev.* **1998**, *98*, 1171.
(31) Burrows, C. J.; Muller, J. G. *Chem. Rev.* **1998**, *98*, 1109. Sigman, D. S.; Mazumder, A.; Perrin, D. M. *Chem. Rev.* **1993**, *93*, 2295.
(32) Pogozelski, W. K.; Tullius, T. D. *Chem. Rev.* **1998**, *98*, 1089.
(33) Roy, M.; Saha, S.; Patra, A. K.; Nethaji, M.; Chakravarty, A. R. *Inorg. Chem.* **2007**, *46*, 4368.
(34) Sreedhara, A.; Cowan, J. A. *J. Biol. Inorg. Chem.* **2001**, *6*, 337.
(35) Wolkenberg, S. E.; Boger, D. L. *Chem. Rev.* **2002**, *102*, 2477.
(36) An, Y.; Liu, S.-D.; Deng, S.-Y.; Ji, L.-N.; Mao, Z.-W. *J. Inorg. Biochem.* **2006**, *100*, 1586.
(37) Sigman, D. S. *Acc. Chem. Res.* **1986**, *19*, 180. Sigman, D. S.; Bruice, T. W.; Mazumder, A.; Sutton, C. L. *Acc. Chem. Res.* **1993**, *26*, 98.
(38) Routier, S.; Vezin, H.; Lamour, E.; Bernier, J.-L.; Catteau, J.-P.; Bailly, C. *Nucleic Acids Res.* **1999**, *27*, 4160.
(39) Fu, P. K.-L.; Bradley, P. M.; van Loyen, D.; Dürr, H.; Bossmann, S. H.; Turro, C. *Inorg. Chem.* **2002**, *41*, 3808.
(40) Van den Berg, T. A.; Feringa, B. L.; Roelfes, G. *Chem. Commun.* **2007**, 180.

Scheme 1. Schematic Drawing of the Complexes and the dpq Ligand

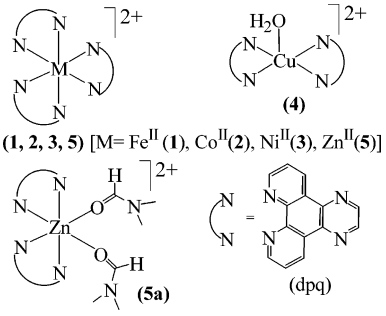

cantly lower dark toxicity in comparison to that of Photofrin.[21,24] The impetus to develop the chemistry of new metal-based phototherapeutic agents stems from the success of the chemotherapeutic drug *cis*-platin and its derivatives.[41,42]

We have recently shown that photoactive organic molecules such as dipyridoquinoxaline (dpq) cleave DNA on irradiation with visible light when bound to a copper(II) center.[26] The quinoxaline moiety, present in antitumor quinoxaline antibiotics, is known to generate photoexcited $^3(n\pi^*)$ and/or $^3(\pi\pi^*)$ state(s) that leads to DNA cleavage by H abstraction and/or electron-transfer pathways.[43] The dpq molecule itself is active in cleaving DNA on exposure to UV-B and UV-C radiation. The same species is, however, cleavage-inactive when irradiated with a visible light or UV-A light of 365 nm. The copper(II) complex of dpq shows efficient DNA cleavage on irradiation with red light in the PDT window of 600−800 nm. The DNA photocleavage at visible light by copper(II) complexes presumably occurs by a metal-assisted process involving d−d band excitation.[25,26] The presence of both the copper(II) center and the photoactive ligand is found to be necessary to observe the red-light-induced DNA cleavage activity. Interestingly, the 1,10-phenanthroline (phen) analogue of the dpq complex is DNA cleavage-inactive in UV and visible light, although both complexes show similar structural characteristics, DNA binding propensities, and redox properties.

The present work stems from our interest in further exploring this chemistry to understand any specific role that is played by the transition-metal ion in exhibiting visible-light-induced DNA cleavage activity. We have chosen bivalent 3d-metal ions such as d^6-iron(II), d^7-cobalt(II), d^8-nickel(II), and d^{10}-zinc(II) in addition to the reported d^9-copper(II) species.[26] The complexes of formulations $[Fe^{II}(dpq)_3](PF_6)_2$ (**1**), $[Co^{II}(dpq)_3](ClO_4)_2$ (**2**), $[Ni^{II}(dpq)_3](ClO_4)_2$ (**3**), $[Cu^{II}(dpq)_2(H_2O)](ClO_4)_2$ (**4**), $[Zn^{II}(dpq)_3](ClO_4)_2$ (**5**), and $[Zn^{II}(dpq)_2(DMF)_2](ClO_4)_2$ (**5a**) (DMF = *N*,*N*-dimethylformamide) were prepared, and their photoinduced DNA cleavage activity was studied (Scheme 1). A significant result of this study is our observation that only the cobalt(II) and copper(II) complexes actively show DNA cleavage activity in visible light. Theoretical studies on the complexes have been made to rationalize the DNA cleavage data in visible light. The results are of importance for the ability to choose suitable 3d-metal ions for the design and development of new metal-based DNA photocleavers for their potential use as PDT agents.

Experimental Section

Materials and Measurements. The reagents and chemicals were procured from commercial sources and used as received without further purification. The solvents used were purified by standard procedures.[44] Supercoiled (SC) pUC19 DNA (cesium chloride purified) was purchased from Bangalore Genie (India). Calf thymus (CT) DNA, agarose (molecular biology grade), distamycin-A, catalase, superoxide dismutase (SOD), 5,5-dimethyl-1-pyrroline *N*-oxide (DMPO), and ethidium bromide (EB) were from Sigma (U.S.A.). Tris(hydroxymethyl)aminomethane−HCl (Tris−HCl) buffer was prepared using deionized and sonicated triple-distilled water. Dipyrido[3,2-d:2′,3′-f]quinoxaline (dpq) was prepared following a literature method.[45] The preparative procedure for complex **4** was reported earlier.[46]

The elemental analysis was done using a Thermo Finnigan FLASH EA 1112 CHNS analyzer. The infrared and electronic spectra were recorded on Perkin-Elmer Lambda 35 and Perkin-Elmer spectrum one 55 spectrophotometers, respectively. Variable-temperature magnetic susceptibility data in the range of of 300−20 K for polycrystalline samples of the complexes were obtained using a model 300 Lewis-coil-force magnetometer of George Associates, Inc. (Berkeley, CA) make. $Hg[Co(NCS)_4]$ was used as a standard. Experimental susceptibility data were corrected for diamagnetic contributions.[47] The molar conductivity measurements were done using a Control Dynamics (India) conductivity meter. Cyclic voltammetric measurements were made at 25 °C using an EG&G PAR 253 VersaStat potentiostat/galvanostat with a three-electrode configuration consisting of a glassy-carbon working electrode, a platinum-wire auxiliary electrode, and a saturated calomel reference (SCE) electrode. Ferrocene ($E_{1/2}$ = 0.42 V) was used as a standard in MeCN−0.1 M $[Bu^n_4N](ClO_4)$ (TBAP). Electrospray ionization mass, electron paramagnetic resonance (EPR), and ^1H NMR spectral measurements were made using Bruker Daltonics (Esquire 300 Plus ESI model), Bruker EMX, and Bruker Avanced 400 NMR spectrometers, respectively. Thermogravimetric experiments were carried out in the temperature range of 30−200 °C using a NETZSCH thermogravimetry analyzer (model TG209F1) coupled with a NETZSCH QMS 403C quadruple mass analyzer.

Preparation of $[Fe(dpq)_3](PF_6)_2$ (1). To 5 mL of an aqueous solution of ammonium ferrous sulfate (0.2 g, 0.5 mmol) was added 10 mL of a methanolic solution of dpq (0.35 g, 1.5 mmol) with stirring for 15 min. The deep-red solution thus obtained was treated with a methanolic solution of NH_4PF_6 (0.17 g, ∼1.0 mmol) to precipitate a red solid that was isolated by filtration and washed with cold methanol followed by diethyl ether and finally dried in vacuum over P_4O_{10} (yield: 0.43 g (∼80%)). The complex was crystallized by a vapor-diffusion technique using an acetonitrile solution of the complex and diethyl ether. Anal. Calcd for $C_{42}H_{24}F_{12}FeN_{12}P_2$: C, 48.39; H, 2.32; N, 16.12. Found: C, 48.53; H, 2.47; N, 15.93. FT-IR (KBr phase, cm^{-1}): 3640w, 3420w, 3086w,

(41) Wang, D.; Lippard, S. J. *Nat. Rev. Drug Discovery* **2005**, *4*, 307.
(42) Barnes, K. R.; Kutikov, A.; Lippard, S. J. *Chem. Biol.* **2004**, *11*, 557.
(43) Toshima, K.; Takano, R.; Ozawa, T.; Matsumura, S. *Chem. Commun.* **2002**, 212.
(44) Perrin, D. D.; Armarego, W. L. F.; Perrin, D. R. *Purification of Laboratory Chemicals*; Pergamon Press: Oxford, 1980.
(45) Collins, J. G.; Sleeman, A. D.; Aldrich-Wright, J. R.; Greguric, I.; Hambley, T. W. *Inorg. Chem.* **1998**, *37*, 3133.
(46) Santra, B. K.; Reddy, P. A. N.; Neelakanta, G.; Mahadevan, S.; Nethaji, M.; Chakravarty, A. R. *J. Inorg. Biochem.* **2002**, *89*, 191.
(47) Khan, O. *Molecular Magnetism*; VCH: Weinheim, Germany, 1993.

1610w, 1488w, 1408m, 1385m, 1259w, 1127w, 1083w, 840vs (PF_6^-), 810s, 732w, 557s, 440w (w, weak; m, medium; s, strong; vs, very strong). ESI-MS in MeCN: *m*/*z* 373 $[M - 2(PF_6^-)]^{2+}$. UV−vis in DMF−Tris HCl buffer (6% DMF) (λ_{max}, nm (ϵ, M^{-1} cm^{-1})): 258 (46 200), 295 (17 900), 331 (2320), 426 (3450), 475sh (4700), 512 (5500) (sh, shoulder). Λ_M (S m^2 M^{-1}) in MeCN: 230.

Preparation of $[Co(dpq)_3](ClO_4)_2$ (2). The complex was prepared from a reaction of 5 mL of an aqueous solution of $[Co(H_2O)_6](NO_3)_2$ (0.15 g, 0.5 mmol) with 10 mL of a methanolic solution of dpq (0.35 g, 1.5 mmol). The resulting solution on refluxing for 15 min gave an orange-red solution. The solution was cooled to an ambient temperature followed by the addition of a methanolic solution of $NaClO_4$ (0.18 g, 1.5 mmol) to obtain an orange-brown precipitate. The solid was collected by filtration, washed with cold methanol followed by diethyl ether, and dried in vacuum over P_4O_{10} (Yield: 0.38 g (∼70%)). Anal. Calcd for $C_{42}H_{24}Cl_2CoN_{12}O_8 \cdot 2H_2O$: C, 50.92; H, 2.85; N, 16.97. Found: C, 51.12; H, 2.61; N, 17.08. The weight loss from TG analysis was 1.8%, which corresponded to a loss of $2H_2O$. FT-IR (KBr phase, cm^{-1}): 3404br, 3078w, 1614w, 1582m, 1481m, 1406s, 1388s, 1309w, 1271w, 1214w, 1088vs (ClO_4^-), 817m, 736s, 624s, 440w (br, broad). ESI-MS in MeCN: *m*/*z* 622 $[(M - (ClO_4^-) - dpq)]^+$. UV−vis in DMF−Tris HCl buffer (6% DMF) (λ_{max}, nm (ϵ, M^{-1} cm^{-1})): 261 (52 900), 325 (22 100), 341 (18 300), 387 (2200), 510 (330), 587 (50). Λ_M in MeCN (S m^2 M^{-1}): 265. μ_{eff} (298 K): 4.60 μ_B.

Preparation of $[Ni(dpq)_3](ClO_4)_2$ (3). Complex **3** was prepared by a procedure similar to that described for **2** using $[Ni(H_2O)_6](NO_3)_2$ (0.15 g, 0.5 mmol), dpq (0.35 g, 1.5 mmol), and $NaClO_4$ (0.12 g, 1 mmol) (Yield: 0.36 g (∼75%)). Anal. Calcd for $C_{42}H_{24}Cl_2N_{12}NiO_8 \cdot 3H_2O$: C, 50.03; H, 3.00; N, 16.67. Found: C, 49.85; H, 2.83; N, 16.53. The weight loss from TG analysis was 5%, which corresponded to a loss of $3H_2O$. FT-IR (KBr phase, cm^{-1}): 3406br, 3074w, 1613w, 1581m, 1406s, 1385s, 1213w, 1087vs (ClO_4^-), 736s, 625s, 440w. ESI-MS in MeCN: *m*/*z* 377 $[M - 2(ClO_4^-)]^{2+}$. UV−vis in DMF−Tris HCl buffer (6% DMF) (λ_{max}, nm (ϵ, M^{-1} cm^{-1})): 261 (41 200), 293 (31 800), 323 (14 100), 338 (13 900), 457 (270), 520 (140), 591 (30). Λ_M (S m^2 M^{-1}) in MeCN: 250. μ_{eff} (298 K): 2.95 μ_B.

Preparation of $[Zn(dpq)_3](ClO_4)_2$ (5) and $[Zn(dpq)_2(DMF)_2](ClO_4)_2$ (5a). To 5 mL of an aqueous solution of $[Zn(H_2O)_6](ClO_4)_2$ (0.19 g, 0.5 mmol) was added a methanolic solution of dpq (0.35 g, 1.5 mmol). The reaction mixture was refluxed for 1 h. The precipitate thus obtained after cooling to an ambient temperature was isolated, washed with cold methanol followed by diethyl ether, and dried in vacuum over P_4O_{10} (Yield: 0.34 g (∼75%)). Anal. Calcd for $C_{42}H_{24}N_{12}Cl_2O_8Zn$: C, 52.49; H, 2.52; N, 17.49. Found: C, 52.22; H, 2.33; N, 17.65. FT-IR (KBr phase, cm^{-1}): 3094br, 1962w, 1613w, 1581m, 1531m, 1482m, 1406s, 1271w, 1212w, 1086vs (ClO_4^-), 814s, 735s, 622m, 438w. ESI-MS in MeCN: *m*/*z* 380.1 $[M - 2(ClO_4^-)]^{2+}$. UV−vis in DMF−Tris HCl buffer (6% DMF) (λ_{max}, nm (ϵ, M^{-1} cm^{-1})): 273 (47 500), 298 (39 100), 337 (7000). Λ_M (S m^2 M^{-1}) in MeCN: 220. ^1H NMR data in DMSO-d_6: δ 9.74 (d, 2H), 9.15 (d, 2H), 8.87 (d, 2H), 8.21 (s, 2H). Complex **5a** in the crystalline form was obtained by a diffusion technique in which a DMF solution of **5** was layered with diethyl ether. The crystals obtained were found to be of formulation $[Zn(dpq)_2(DMF)_2](ClO_4)_2$. Anal. Calcd for $C_{34}H_{30}N_{10}Cl_2O_{10}Zn$: C, 46.67; H, 3.46; N, 16.01. Found: C, 46.49; H, 3.31; N, 16.19. FT-IR (KBr phase, cm^{-1}): 3420br, 3080w, 2930w, 1650m, 1580w, 1530w, 1490m, 1413m, 1383s, 1214w, 1088vs (ClO_4^-), 823s, 734s, 625m, 425w. UV−vis in DMF−Tris HCl buffer (6% DMF) (λ_{max}, nm (ϵ, M^{-1} cm^{-1})): 270 (48 100), 302 (40 300), 340 (7600). Λ_M (S m^2 M^{-1}) in MeCN: 240.

Solubility and Stability. The complexes showed good solubility in MeCN, DMSO, and DMF and moderate solubility in aqueous DMF. The Co^{II} complex showed the loss of one dpq ligand during mass spectral analysis in MeCN. The complex, however, did not show any loss of dpq ligand during cyclic voltammetry in MeCN−TBAP. The Zn^{II} complex **5** in DMF was found to form a bis-DMF adduct (**5a**) during crystallization with the loss of one dpq ligand. Complex **5a** was used for DNA binding and cleavage studies. As perchlorate salts of the metal complexes are potentially explosive, only a small quantity of material in the samples was used, with necessary precautions.

X-ray Crystallographic Procedures. Crystals of **1** and **5a** were mounted on glass fibers with epoxy cement, and the X-ray diffraction data were measured in frames with increasing ω (width of 0.3° per frame) and with a scan speed at 15 s/frame using a Bruker SMART APEX CCD diffractometer, equipped with a fine-focus 1.75 kW sealed-tube X-ray source. Empirical absorption corrections were made using a multiscan program.[48] The structure was solved by the heavy-atom method and refined by full matrix least squares using the *SHELX* system of programs.[49] The perspective views of the complexes were obtained using the *ORTEP* program.[50] There were two molecules in the crystallographic asymmetric unit of **1** in the monoclinic space group *C*2/*c*. The angles observed between the dpq ligands in two independent molecules belonging to the crystallographic asymmetric unit differed considerably from each other (82° for molecule A and 85° for molecule B). While three PF_6 anions in **1** were refined with full occupancy, one positionally disordered PF_6 anion was modeled for two PF_6 units, each refined with half-occupancy. One PF_6 anion was found in the special position. The non-hydrogen atoms were refined anisotropically, except the disordered ones. The crystal structure of **5a** also showed the presence of two molecules in the crystallographic asymmetric unit belonging to the space group $P2_1/c$. Both structures refined well without showing any unusual features.

DNA Binding and Cleavage Experiments. DNA binding experiments were done in Tris−HCl/NaCl buffer (5 mM Tris−HCl, 5 mM NaCl, pH 7.2) using DMF solution of the complexes **1**−**4** and **5a**. CT DNA (ca. 250 μM NP) in a Tris−HCl buffer medium gave a UV absorbance ratio of ca. 1.9:1 at 260 and 280 nm, suggesting that the DNA was apparently free from any protein impurity. The concentration of CT DNA was measured from its absorption intensity at 260 nm using a molar absorption coefficient value of 6600 M^{-1} cm^{-1}.[51] Absorption titration experiments were made using different concentrations of CT DNA, keeping the metal complex concentration constant with due correction for the absorbance of the CT DNA itself. Samples were equilibrated before recording each spectrum. The equilibrium binding constant (*K*) and the binding site size (*s*) of the complex were determined from a nonlinear fitting of the plot of $\Delta\epsilon_{af}/\Delta\epsilon_{bf}$ vs [DNA] applying the McGhee−von Hippel method and using the expression of Bard and co-workers, $C_b = (b - (b^2 - 2K^2C_t[DNA]/s)^{1/2})/2K$, $b = 1 + KC_t + K[DNA]/2s$, where *K* is the microscopic binding constant for each site, C_b is the concentration of the DNA-bound complex, C_t is the total concentration of the metal complex, and *s* is the site size (in base pairs) of the metal complex interacting with the DNA and ϵ_f, ϵ_a, and ϵ_b are respectively the molar extinction coefficients of the

(48) Walker, N.; Stuart, D. *Acta Crystallogr.* **1993**, *A39*, 158.
(49) Sheldrick, G. M. *SHELX-97, Programs for Crystal Structure Solution and Refinement*; University of Göttingen: Göttingen, Germany, 1997.
(50) Johnson, C. K. *ORTEP*; Report ORNL-5138; Oak Ridge National Laboratory: Oak Ridge, TN, 1976.
(51) Reichman, M. E.; Rice, S. A.; Thomas, C. A.; Doty, P. *J. Am. Chem. Soc.* **1954**, *76*, 3047.

Table 1. Selected Physicochemical Data for the Complexes **1**−**4** and **5a**

	complex				
	1	**2**	**3**	**4**	**5a**
visible band: λ_{max}/nm (ϵ/M^{-1} cm^{-1})[a]	512 (5500), 475 (4700)	587 (50), 510 (330)	591 (30), 520 (140)	673 (70)[b]	
Λ_M[c]/S m^2 M^{-1}	230	265	250	255	240
CV: $E_{1/2}$/V (ΔE_p/mV)[d]	1.2 (80)[e] [Fe^{III}/Fe^{II}]	0.4(100)[f] [Co^{III}/Co^{II}]	[g]	0.09 (100)[b,h] [Cu^{II}/Cu^{I}]	[i]
μ_{eff} /μ_B[j]		4.6	2.95	1.81	
K/M^{-1} [s][k]	3.1(±0.7) × 10^5 [0.44]	2.3(±0.5) × 10^5 [0.32]	3.8(±0.6) × 10^5 [0.54]	5.4(±0.3) × 10^5 [0.48]	4.9(±0.7) × 10^5 [0.44]
ΔT_m[l]/°C	2.5 ± 0.1	2.1 ± 0.1	2.1 ± 0.1	2.5 ± 0.1	2.3 ± 0.1

[a] In DMF−Tris−HCl buffer (pH 7.2). [b]Ref 26. [c] Molar conductance in MeCN. [d] Metal-based redox process in DMF−0.1 M TBAP, $E_{1/2} = 0.5(E_{pa} + E_{pc})$, $\Delta E_p = E_{pa} - E_{pc}$, where E_{pa} and E_{pc} are the anodic and cathodic peak potentials, respectively. Scan rate = 50 mV s^{-1}. The potentials are versus SCE. [e]Additional cathodic peaks at −1.25 and −1.6 V with a weak anodic response at −1.3 V. The dpq ligand alone showed cathodic peaks at −1.2 and −1.65 V with a weak anodic counterpart at −0.67 V. [f] Additional cathodic peaks at −1.3 and −1.6 V with a weak anodic counterpart at −1.1 V. [g] Showed no metal-based redox process. Cathodic peaks at −1.35 and −1.6 V with a weak anodic response at −1.0 V. [h] Additional cathodic peaks at −1.3 and −1.55 V with a weak anodic response at −1.1 V. [i]Showed no metal-based redox process. Irreversible ligand reductions were observed at −1.2 and −1.6 V with a weak anodic response at −1.3 V. [j]Magnetic moments at room temperature (298 K) for powdered solid samples. The Fe^{II} and Zn^{II} complexes are diamagnetic. [k]Intrinsic binding constant from McGhee−von Hippel method with "*s*" as the binding site size. [l] Change in the DNA melting temperature.

free complex in solution, the complex bound to DNA at a definite concentration, and the complex in a completely bound form with CT DNA.[52,53] The nonlinear least-squares analysis was done using *Origin Lab*., version 6.1.

DNA-denaturation experiments were carried out by monitoring the absorbance of CT DNA (260 nm) at various temperatures in the absence and presence of the complexes in a 20:1 molar ratio of CT DNA and the complex with a ramp rate of 0.5 °C min^{-1} in 5 mM phosphate-buffer medium (pH 6.85) using a Cary 300 bio UV−vis spectrometer with a Cary temperature controller. The viscosity measurements were done using a Schott Gerate AVS 310 automated viscometer attached to a constant temperature bath at 37 °C. The concentration of CT DNA stock solution was 130 μM (NP) in a 5 mM Tris−HCl buffer. The complex was added gradually in increasing concentration from 0 to 120 μM, and the viscosity was measured for each addition. The flow times were monitored with an automated timer. The data were presented by plotting the relative specific viscosity of DNA, $(\eta/\eta_0)^{1/3}$ vs [complex]/[DNA], where η is the viscosity of DNA in the presence of complex and η_0 is the viscosity of DNA alone in 5 mM Tris buffer medium. The viscosity values were calculated from the observed flow time of CT DNA containing solutions (t), duly corrected for that of the buffer alone (t_0), $\eta = (t - t_0)$.

The photoinduced cleavage of SC pUC19 DNA by the 3d-metal complexes **1**−**4** and **5a** was studied by agarose gel electrophoresis. The reactions were carried out under illuminated conditions using a UV lamp of 365 nm (12 W, sample area of illumination, 45 mm^2) and at different visible wavelengths using a continuous-wave (CW) argon−krypton laser of 50 mW laser power, laser beam diameter of 1.8 mm with a beam divergence of 0.70 mrad of the Spectra Physics water-cooled mixed-gas ion laser stabilite 2018-RM. The power of the laser beam at the sample position was measured using Spectra Physics CW laser power meter (model 407A). Eppendorf and glass vials were used for respective UV and visible light experiments in a dark room at 25 °C using SC DNA (1 μL, 33.3 μM) in 50 mM Tris−HCl buffer (pH 7.2) containing 50 mM NaCl and the complex (2 μL) with varied concentrations. Different additives were used for mechanistic investigations in the presence of the 3d-metal complexes prior to light exposure. The concentration of the complexes in DMF or the additives in buffer corresponded to the quantity in 2 μL stock solution after dilution to the 18 μL final volume using Tris−HCl buffer. The solution path length in the sample vial was ∼5 mm. After the photoexposure, the sample was incubated for 1 h at 37 °C, followed by its addition to the loading buffer containing 25% bromophenol blue, 0.25% xylene cyanol, and 30% glycerol (3 μL). The solution was finally loaded on 0.8% agarose gel containing 1.0 μg mL^{-1} of EB. Electrophoresis was carried out in a dark room for 2 h at 45 V in Tris−acetate−EDTA buffer. The bands were visualized by UV light and photographed. The extent of DNA cleavage was determined by measuring the intensities of the bands using a UVITECH gel documentation system. Due corrections were made for the presence of a minor quantity of nicked circular (NC) in the original SC DNA sample and for the low affinity of EB binding to SC compared with that of NC and linear forms of DNA.[54] The extent of experimental error in measuring the SC and NC forms of DNA from the gel diagram varied from 3 to 5%.

Results and Discussion

Synthesis and General Aspects. Bivalent 3d-metal complexes **1**−**5** and **5a** of the dpq ligand are prepared in good yield and characterized from analytical, spectral, and magnetic data (Scheme 1 and Table 1). The Zn^{II} complex **5** forms a bis-DMF adduct (**5a**) when crystallized from a DMF solution of the complex. All the complexes are 1:2 electrolytic in MeCN. They show characteristic infrared bands for the PF_6/ClO_4 anions. Magnetic susceptibility measurements on the solid samples of the complexes show diamagnetic nature of the $3d^6$-iron^{II} [$t_{2g}^6e_g^0$] complex **1**, while $3d^7$-Co^{II}, $3d^8$-Ni^{II}, and $3d^9$-Cu^{II} complexes (**2**−**4**) are paramagnetic, having three [$t_{2g}^5e_g^2$], two [$t_{2g}^6e_g^2$] and one unpaired electron(s), respectively. The electronic spectra of the complexes in Tris−HCl buffer containing 6% DMF (pH 7.2) display two visible bands near 512 and 475 nm for **1**, assignable to metal-centered charge-transfer transitions (Figure 1). In addition, a visible band is observed at 423 nm. The Co^{II} complex exhibits metal-centered bands at 587 and 510 nm assignable to $^4T_{2g} \leftarrow {}^4T_{1g}$ and $^4A_{2g} \leftarrow {}^4T_{1g}$ transitions. The Ni^{II} complex shows two visible bands at 591 and 520 nm, and they are assigned to $^3T_{2g} \leftarrow {}^3A_{2g}$ and $^3T_{1g} \leftarrow {}^3A_{2g}$ transitions. An

(52) McGhee, J. D.; von Hippel, P. H. *J. Mol. Biol.* **1974**, *86*, 469.
(53) Carter, M. T.; Rodriguez, M.; Bard, A. J. *J. Am. Chem. Soc.* **1989**, *111*, 8901.
(54) Bernadou, J.; Pratviel, G.; Bennis, F.; Girardet, M.; Meunier, B. *Biochemistry* **1989**, *28*, 7268.

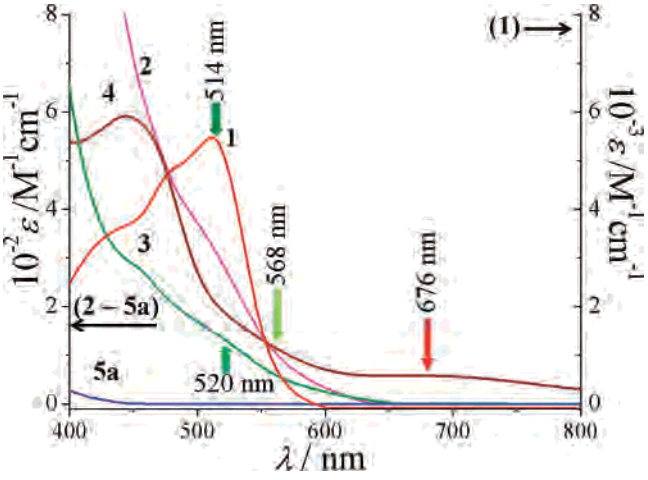

Figure 1. Electronic spectra of the complexes **1**−**4** and **5a** in Tris−HCl buffer (pH 7.2) containing 6% DMF (color code: **1** (red), −**2** (pink), −**3** (green), −**4** (brown), and −**5a** (blue)). The arrows indicate the wavelengths of the light used for photoirradiation of DNA.

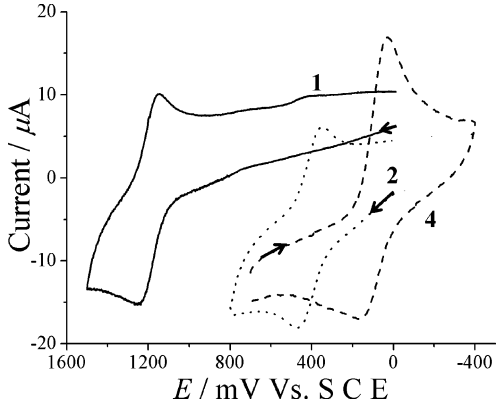

Figure 2. Cyclic voltammograms showing the metal-based redox processes in the complexes **1**, **2**, and **4** in DMF−0.1 M TBAP (scan rate: 50 mV s^{-1}).

additional visible band is observed at 457 nm for this complex. The diamagnetic $3d^{10}$-Zn^{II} complex does not show any visible spectral band. The d−d band in the Cu^{II} complex is observed at 673 nm.[26] The spectral bands due to n−π^* and π−π^* electronic transitions of the dpq ligand are observed in the UV region.[43]

The Fe^{II}, Co^{II}, and Cu^{II} complexes display metal-based quasi-reversible cyclic voltammetric responses in DMF−0.1 M TBAP (Figure 2). The Fe^{III}/Fe^{II} couple in **1** is observed at 1.2 V vs SCE. Such a high redox potential renders stability to the Fe^{II} state in **1** with a low-spin electronic configuration. The cobalt(II) complex undergoes oxidation at a significantly lower potential, giving an $E_{1/2}$ value of 0.4 V for the Co^{III}/Co^{II} couple. Complexes **3** and **5a** do not show any metal-based redox process, suggesting the stability of the bivalent metal oxidation state in the Ni^{II} and Zn^{II} species. The Cu^{II} complex **4** undergoes reduction to the Cu^{I} species giving an $E_{1/2}$ value of 0.09 V for the Cu^{II}/Cu^{I} couple.[26] The peak-to-peak separations (ΔE_p) of 80−100 mV at 50 mV s^{-1} scan rate with a i_{pa}/i_{pc} ratio of unity suggest the quasi-reversible nature of the electron-transfer processes for the metal-based redox couples (i_{pa} and i_{pc} are anodic and cathodic peak currents, respectively). All the complexes show two cathodic peaks in the potential range of −1.2 to −1.7 V with an anodic peak of significantly reduced peak current near −1.1 V. These irreversible cyclic voltammetric responses are assignable to the dpq ligand, as a similar redox behavior is observed for the free dpq.

The Fe^{II} and Zn^{II} complexes **1** and **5a** were structurally characterized by the single-crystal X-ray diffraction technique. The crystal structure of the Cu^{II} complex was reported earlier.[46] Complexes **1** and **5a** crystallize in the respective *C*2/*c* and $P2_1/c$ space groups belonging to the monoclinic crystal system. The molecular structure of **1** consists of an iron(II) center bound to three bidentate chelating dpq ligands giving an essentially octahedral FeN_6 coordination and two PF_6 anions per formula unit. The average Fe−N(dpq) distance is 1.977(2) Å. The molecular structure of **5a** shows the zinc(II) center bound to two bidentate chelating dpq ligands and two DMF ligands in cis disposition giving a distorted ZnN_4O_2 coordination. There are two perchlorate anions per formula unit. The average Zn−N(dpq) and Zn−O(DMF) distances are 2.160(6) and 2.087(3) Å, respectively. Selected crystal data, important bond distances and angles, the ORTEP views, and unit cell packing diagrams for **1** and **5a** are given as Supporting Information (Tables S1−S3 and Figures S1−S4).

DNA Binding Studies. The binding properties of the 3d-metal complexes to CT DNA are studied using various techniques (Table 1). Absorption spectral measurements are carried out to determine the equilibrium binding constant (*K*) and binding site size (*s*) of the complexes to CT DNA by monitoring the change in the absorption intensity of the spectral band at ∼340 nm for all the complexes. Complexes **1**−**4** and **5a** show minor bathochromic shift of the spectral band of ∼2 nm suggesting a groove-binding preference of the complexes (Figure S5, Supporting Information). The *K* and *s* values of the complexes are in the ranges of 3.0×10^5 to 5.0×10^5 M^{-1} and 0.3−0.5, respectively. The Cu^{II} and Zn^{II} complexes show higher binding propensity than their octahedral Fe^{II}, Co^{II}, and Ni^{II} analogues due to structural differences. The *K* values of the dpq complexes compare well with those of other known transition-metal complexes of the dpq ligand but are less than those of the dipyridophenazine (dppz) analogues.[20] This is because of the presence of an extended aromatic ring in dppz that facilitates its potential intercalative and/or DNA major groove binding, while dpq prefers to bind at the DNA minor groove. The binding site size (*s*) that gives a measure of the number of DNA bases associated with the complex is in the range of 0.3−0.5, suggesting the DNA groove-binding nature of the complexes in preference over that of intercalation. A low value of *s* (≤1) is suggested for an aggregation of hydrophobic molecules on the DNA surface due to π stacking.[55] The dpq ligand with its extended quinoxaline aromatic ring could undergo π-stacking interactions with the DNA.

DNA melting experiments show only a minor shift in the melting temperature (T_m) giving a ΔT_m value of ∼2.0 °C on the addition of the complexes to CT DNA (Figure S6,

(55) Nair, R. B.; Teng, E. S.; Kirkland, S. L.; Murphy, C. J. *Inorg. Chem.* **1998**, *37*, 139.

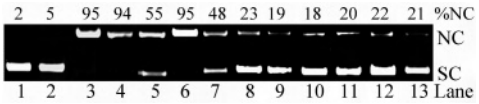

Figure 3. Gel electrophoresis diagram showing the extent of cleavage of SC pUC19 DNA (0.2 μg, 33.3 μM) by the complexes **1**−**4** and **5a** (5.5 μM) in 50 mM Tris−HCl/NaCl buffer (pH, 7.2) containing 6% DMF in UV light of 365 nm (12 W) for an exposure time of 2.0 h: lane 1, DNA control; lane 2, DNA + dpq (33.3 μM); lane 3, DNA + **1**; lane 4, DNA + **2**; lane 5, DNA + **3**; lane 6, DNA + **4**; lane 7, DNA + **5a**; lane 8, DNA + distamycin-A; lane 9, DNA + distamycin-A + **1**; lane 10, DNA + distamycin-A + **2**; lane 11, DNA + distamycin-A + **3**; lane 12, DNA + distamycin-A + **4**; lane 13, DNA + distamycin-A + **5a**.

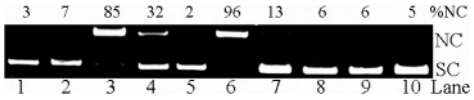

Figure 4. Gel electrophoresis diagram showing the visible-light-induced cleavage of SC pUC19 DNA (0.2 μg, 33.3 μM) by the complexes **1**−**4** and **5a** (10.1 μM) at wavelengths 514, 520, 568, and 676 nm (50 mW CW Ar−Kr laser power) in 50 mM Tris−HCl/NaCl buffer (pH, 7.2) with a 2.0 h photoexposure time: lane 1, DNA control (514 nm); lane 2, DNA + **1** (514 nm); lane 3, DNA + **2** (514 nm); lane 4, DNA + **3** (520 nm); lane 5, DNA control (676 nm); lane 6, DNA + **4** (676 nm); lane 7, DNA + **5a** (514 nm); lane 8, DNA + **5a** (520 nm); lane 9, DNA + **5a** (568 nm); lane 10, DNA + **5a** (676 nm).

Supporting Information). The data suggest a primarily groove-binding nature of the complexes. The complexes having good intercalating ligands are known to show significantly high ΔT_m values.[56] To further explore the DNA binding propensity of the complexes, viscosity measurements were carried out. A significant increase in the viscosity of DNA on the addition of any external species indicates the intercalative mode of binding to DNA. In contrast, compounds binding to DNA grooves result in minor variation or no variation in the viscosity of the DNA solution. The plot of $(\eta/\eta_0)^{1/3}$ vs [complex]/[DNA] gives a measure of the viscosity changes (Figure S7, Supporting Information). A marginal increase of the relative viscosity is observed on the addition of the present complexes to the DNA solution, suggesting the groove-binding nature of the complexes.

DNA Photocleavage. The photoinduced DNA cleavage activity of the 3d-metal complexes is studied using SC pUC19 DNA (33.3 μM, 0.2 μg) in a medium of Tris−HCl/NaCl (50 mM, pH, 7.2) buffer on irradiation with a low power monochromatic UV light of 365 nm (12 W) and monochromatic visible light of wavelengths 514, 520, 568, and 676 nm (50 mW) using a CW argon−krypton mixed-gas ion laser. The extent of DNA cleavage from SC to the nicked circular (NC) form is shown in Figures 3−5 (gel electrophoresis diagrams are seen in Figures 3 and 4; see also Figures S8−S11, Supporting Information). Selected DNA cleavage data are given in Table 2. The cleavage activity at 365 nm follows the order: **4** [Cu^{II}] > **2** [Co^{II}] > **1** [Fe^{II}] > **3** [Ni^{II}] ≥ **5a** [Zn^{II}] (Figure 3). A 5.5 μM concentration of the complexes **1**, **2**, and **4** shows essentially complete cleavage of SC DNA for an exposure time of 2 h. The complexes **3** and **5** are found to be less active under similar reaction conditions. The UV-light-induced DNA cleavage is likely to involve the dpq ligand, having a quinoxaline moiety with conjugated C=N bonds that could generate photoexcited $^3(n-\pi^*)$ and/or $^3(\pi-\pi^*)$ state(s) effecting DNA cleavage following an oxidative pathway.[43] Control experiments show that the metal salts $(NH_4)_2Fe(SO_4)_2$, $[Co(H_2O)_6](NO_3)_2$, $[Ni(H_2O)_6](NO_3)_2$, $[Cu(H_2O)_6](ClO_4)_2$, and $[Zn(H_2O)_6](ClO_4)_2$ (10.1 μM) alone do not show any significant photocleavage of DNA at 365 nm. Again, the complexes in dark or the dpq ligand (33.3 μM) alone on photoexposure do not show any appreciable DNA cleavage activity. On the basis of the cleavage data, we propose the involvement of the metal-to-ligand charge transfer (MLCT) band(s) in the photoexcitation process.

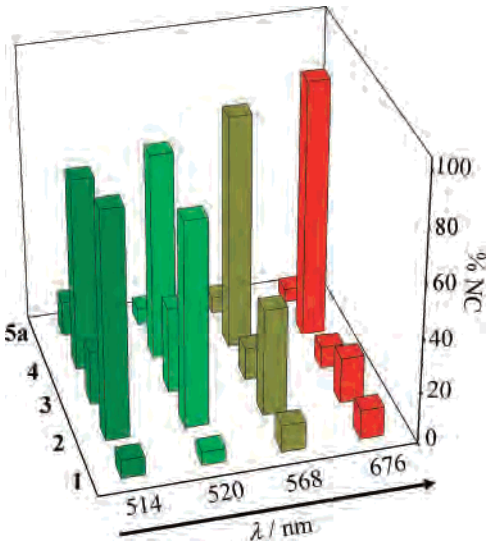

Figure 5. Comparison of the SC pUC DNA (0.2 μg, 33.3 μM) cleavage activity of the complexes **1**−**4** and **5a** (10.1 μM) at visible wavelengths (514, 520, 568, and 676 nm) in 50 mM Tris−HCl/NaCl buffer (pH 7.2) with 50 mW laser power for an exposure time of 2.0 h.

Table 2. Selected Data on the Photoinduced Cleavage of pUC19 DNA (0.2 μg, 33.3 μM) by the Complexes **1**−**4** and **5a** in DMF−Tris Buffer

Sl No.	reaction condition	λ/nm [t/h][a]	NC (%)
1	DNA control	365 [2]	2
2	DNA + dpq (33.3 μM)	365 [2]	5
3	DNA + **1** [Fe^{II}]	365 [2]	95
4	DNA + **2** [Co^{II}]	365 [2]	94
5	DNA + **3** [Ni^{II}]	365 [2]	55
6	DNA + **4** [Cu^{II}]	365 [2]	95
7	DNA + **5a** [Zn^{II}][b]	365 [2]	48
8	DNA control	514 [2]	3
9.	DNA + **1** [Fe^{II}]	514 [2]	7
10	DNA + **2** [Co^{II}]	514 [2]	85
11	DNA + **3** [Ni^{II}]	520 [2]	32
12	DNA + **4** [Cu^{II}]	676 [2]	96

[a] Complex concentration: 5.5 μM at 365 nm and 10.1 μM in visible light experiments; t, photoexposure time. [b] SC DNA cleavage observed for the Zn^{II} complex **5a** at 514, 520, and 676 nm is in the range of 6−10%.

The complexes on photoexposures at visible wavelengths of 514, 520, 568, and 676 nm from a tunable CW Ar−Kr laser (50 mW laser power) show an interesting trend in the DNA cleavage activity (Table 2 and Figure 4). The choice of these wavelengths for photoirradiation is based on the presence of the metal-centered bands at ~510 nm for **1**−**3**, ~590 nm for **2** and **3**, and 673 nm for **4**. We have earlier reported the DNA cleavage activity of the Cu^{II} complex **4** under red light using a 633 nm He−Ne laser and a 694 nm

(56) Fu, P. K.-L.; Bradley, P. M.; Turro, C. *Inorg. Chem.* **2003**, *42*, 878.

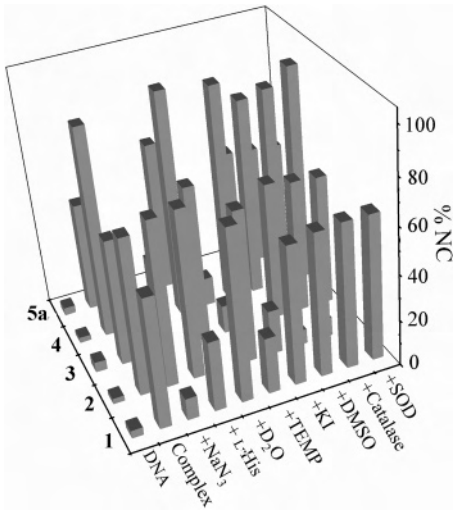

Figure 6. 3D diagram showing SC pUC19 DNA (0.2 μg, 33.3 μM) cleavage data for the complexes **1**−**4** and **5a** in 50 mM Tris−HCl−NaCl buffer (pH 7.2) in UV light of 365 nm (1.0 h photoexposure time for the complexes **1**, **2**, and **4** and 2.0 h exposure time for **3** and **5a**).

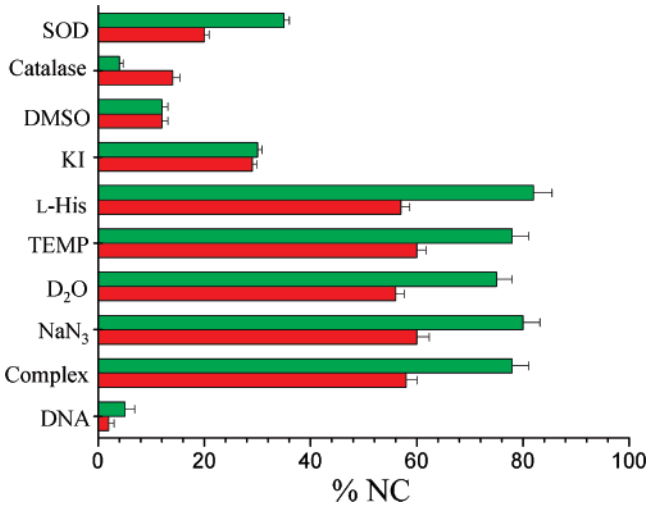

Figure 7. Mechanistic data for the photoinduced cleavage of SC pUC19 DNA (0.2 μg, 33.3 μM) in 50 mM Tris−HCl/NaCl (pH 7.2) buffer by the complexes **2** (green) and **4** (red) at 514 and 676 nm, respectively (complex concentration, 10.1 μM; photoexposure time, 1.0 h).

ruby laser.[26] Complex **5a** with a d^{10}-Zn^{II} center does not show any visible-light-induced DNA cleavage activity at these wavelengths. The diamagnetic Fe^{II} complex **1** is found to be cleavage-inactive on excitation of its MLCT band at 512 nm, having a high molar extinction coefficient value. The paramagnetic Ni^{II} complex **3** shows poor photoinduced DNA cleavage activity on exposure, at its d−d band at 520 nm. In contrast, the paramagnetic Co^{II} (**2**) and Cu^{II} (**4**) complexes display efficient DNA photocleavage activity on excitation at their visible band. A comparison of the visible-light-induced DNA cleavage activity of the complexes is shown in Figure 5. The DNA cleavage activity at visible light follows the order: **4** [Cu^{II}] > **2** [Co^{II}] ≫ **3** [Ni^{II}] ≫ **1**[Fe^{II}], **5a** [Zn^{II}]. The diamagnetic Fe^{II} and Zn^{II} complexes are essentially cleavage-inactive at visible wavelengths.

The mechanistic aspects of the photoinduced DNA cleavage activity of **1**−**4** and **5a** are investigated using various additives at UV and visible wavelengths (Figures 6 and 7).

Scheme 2. Mechanistic Pathways Involved in the Photoinduced DNA Cleavage Reactions

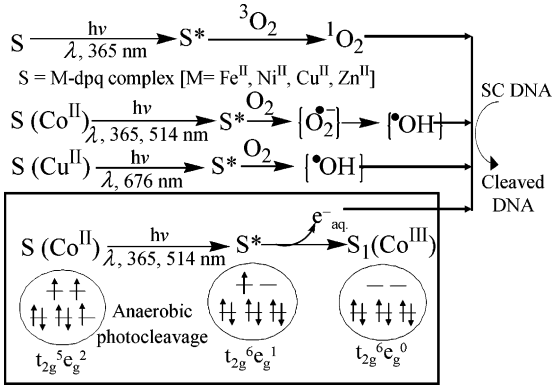

The addition of singlet oxygen quencher sodium azide or TEMP significantly reduces the DNA cleavage activity at 365 nm for the complexes **1**, **3**, **4**, and **5a**. Hydroxyl radical scavangers such as DMSO and KI have no apparent effect on the DNA cleavage activity of the Fe^{II}, Ni^{II}, Cu^{II}, and Zn^{II} complexes at this wavelength. Hydrogen peroxide and superoxide scavengers like catalase and SOD do not show any apparent effect on the DNA cleavage activity. The results suggest the involvement of singlet oxygen ($^1O_2$) in the photocleavage reaction at 365 nm for **1**, **3**, **4**, and **5a**. The involvement of $^1O_2$ is indicated from the enhancement of the DNA cleavage activity in D_2O. This could be due to the longer lifetime of $^1O_2$ in D_2O compared with that in water.[57] The DNA cleavage reaction involving molecular oxygen ($^3O_2$) seems to proceed via a type-2 process in which the singlet excited electronic state of the complex, through efficient intersystem crossing, could generate the triplet excited state of the photosensitizer (complex) that activates molecular oxygen from its stable triplet to the reactive singlet $^1O_2$ ($^1\Delta_g$) state (Scheme 2). Sodium azide, TEMP, and D_2O do not show any apparent effect on the DNA cleavage activity of the Co^{II} complex **2**, while the addition of hydroxyl radical scavengers such as KI, DMSO, hydrogen peroxide scavenger catalase, and the superoxide radical scavenger SOD significantly inhibits DNA cleavage activity. It appears that the DNA cleavage activity at 365 nm proceeds via a photoredox pathway for the cobalt(II) complex, while it is a singlet oxygen pathway for the other complexes.[58] We have studied the groove-binding preference of the complexes using DNA minor groove binder distamycin-A that alone shows ∼20% cleavage of the SC DNA at 365 nm for an exposure time of 2 h. The addition of the dpq complexes (5.5 μM) to distamycin-A-bound DNA shows no significant change in the DNA cleavage activity, suggesting the minor groove-binding propensity of the complexes.

Mechanistic studies at visible light are done using cleavage-active Co^{II} and Cu^{II} complexes at laser wavelengths of 514 and 676 nm, respectively (Figure 7). Addition of singlet oxygen quenchers does not show any apparent change in

(57) Khan, A. U. *J. Phys. Chem.* **1976**, *80*, 2219. Merkel, P. B.; Kearns, D. R. *J. Am. Chem. Soc.* **1972**, *94*, 1029.
(58) Collet, M.; Hoebeke, M.; Piette, J.; Jakobs, A.; Lindqvist, L.; Van der Vorst, A. *J. Photochem. Photobiol., B* **1996**, *35*, 221.

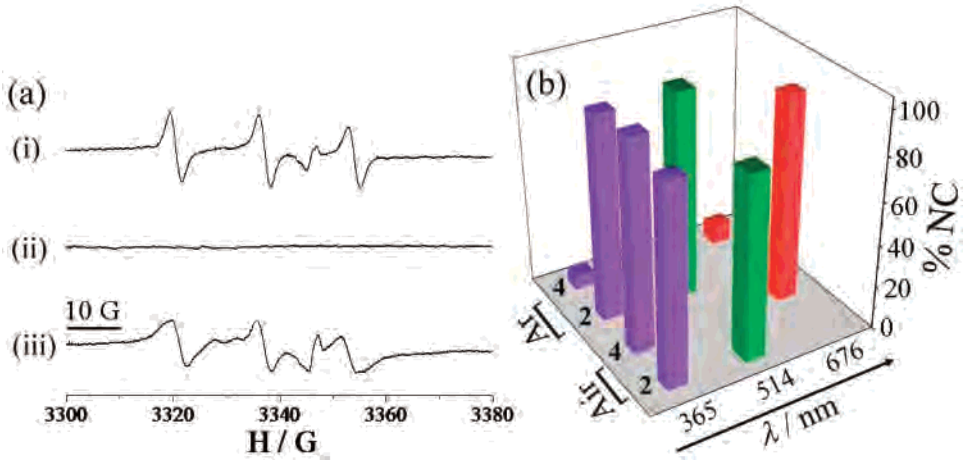

Figure 8. (a) (i) EPR spectrum of complex **2** (100 μM) at 298 K in DMF−Tris−HCl buffer, (ii) EPR spectrum of **2** recorded after UV exposure at 365 nm for 1.0 h, and (iii) EPR spectrum of **2** in the dark recorded 1 h after photoexposure at 365 nm. (b) 3D diagram showing the photocleavage of SC pUC19 DNA (0.2 μg, 33.3 μM) by the complexes **2** and **4** at 365 nm and in visible light of 514 nm for Co^{II} and 676 nm for Cu^{II} under an argon atmosphere (complex concentration: 5.5 μM in UV and 10.1 μM in visible light). The DNA cleavage values for **2** are 62 and 80% , respectively, in air and argon for an exposure time of 1.0 h at 365 nm.

the DNA photocleavage activity of both **2** and **4**. However, hydroxyl radical scavengers such as KI, DMSO, and catalase significantly inhibit the DNA photocleavage activity of the complexes, suggesting the involvement of the hydroxyl radical as a cleavage-active species. Addition of SOD also reduces the DNA photocleavage activity, showing significant inhibition for the Co^{II} complex. The results indicate the formation of hydroxyl radical via a photoredox pathway. Complex **2** with an accessible Co^{III}/Co^{II} redox couple at 0.4 V (vs SCE in DMF−0.1 M TBAP) could undergo an electron transfer from metal to molecular oxygen on photoexcitation to form EPR-inactive Co^{III} and an active oxygen species, which could be the highly reactive superoxide radical that is susceptible to conversion to the hydroxyl radical by the reaction $O_2^{\bullet-} + 2H_2O \rightarrow H_2O_2 + HO^- + HO^{\bullet}$ (Scheme 2). Complex **2** is EPR-active (Figure 8a). On exposure to the UV light of 365 nm for 1 h, it becomes EPR-inactive. On keeping the sample in the dark for 1 h after photoexposure, the EPR signals of **2** reappear (Figure 8a). In the presence of DMPO, the EPR signals that could be due to the formation of the hydroxyl radical are observed on photoexposure of the sample at 365 nm (Figure S13, Supporting Information).[59] The photoredox pathway is also feasible for the Cu^{II} complex that has an accessible redox potential for the Cu^{II}/Cu^{I} couple. It enables the conversion of the $3d^9$-Cu^{II} to $3d^{10}$-Cu^{I} species on photoexcitation at 676 nm by an electron transfer to the metal center in the excited state. The Cu^{I} species is known to activate molecular oxygen to produce a hydrogen peroxide/superoxide that subsequently converts to reactive hydroxyl radical.[60] While the mechanistic pathway for the Co^{II} species involves hydroxyl radical formation at both 365 and 514 nm, the mechanistic pathways for the Cu^{II} complex involve singlet oxygen and hydroxyl radical formation at 365 and 676 nm, respectively. The difference could be related to the redox behavior of the complexes (Figure 2 and Supporting Information Figure S12).

The DNA cleavage activity is also studied under anaerobic conditions in argon. While the Cu^{II} complex is cleavage-inactive at both 365 and 676 nm, the Co^{II} complex shows efficient DNA cleavage activity at 365 and 514 nm under argon atmosphere (Figure 8). The Co^{II} complex is believed to undergo photoionization to Co^{III} by the process $\mathbf{2} + h\nu \rightarrow \mathbf{2}^* \rightarrow \mathbf{2}^+ + e_{aq}^-$. The hydrated electron could lead to DNA damage in a method similar to that reported by Fukuzumi and co-workers for the reductive DNA cleavage induced by UV irradiation of NADH under N_2 at 355 nm.[61] The DNA cleavage possibly takes place due to the initial reduction of nucleobases followed by H abstraction from the deoxyribose moiety.[62] Our observation of better DNA cleavage activity under argon than air suggests quenching of the aquated electron by molecular oxygen to form reactive $O_2^{\bullet-}$ that also causes DNA damage, besides generating the hydroxyl radical. The Co^{II} complexes are known to exhibit valence tautomerization in which the high-spin Co^{II} species on photoirradiation undergoes facile conversion to the Co^{III} species and the electron is either transferred to the metal-bound ligand in quinone complexes or to the substrate molecule such as DNA in our case.[63]

Computational Studies. We have carried out DFT calculations (BP86/LANL2DZ) to further understand the experimental results.[64] The geometrical parameters obtained

(59) Sakurai, H.; Miki, T.; Imakura, Y.; Shibuya, M.; Lee, K.-H. *Mol. Pharmacol*. **1991**, *40*, 965.

(60) Thederahn, T. B.; Kuwabara, M. D.; Larsen, T. A.; Sigman, D. S. *J. Am. Chem. Soc.* **1989**, *111*, 4941. Zelenko, O.; Gallagher, J.; Sigman, D. S. *Angew. Chem., Int. Ed. Engl.* **1997**, *36*, 2776.

(61) Tanaka, M.; Ohkubo, K.; Fukuzumi, S. *J. Am. Chem. Soc.* **2006**, *128*, 12372. Sortino, S.; Giuffrida, S.; Scaiano, J. C. *Chem. Res. Toxicol.* **1999**, *12*, 971.

(62) The 1,10-phenanthroline (phen) complex of Co^{II}, viz. $[Co(phen)_3]^{2+}$ shows visible-light-induced DNA cleavage activity at 514 nm. A 10.1 μM solution of the complex shows ~45 % cleavage of SC pUC19 DNA to its NC form after 2 h of photoexposure. In contrast, the analogous bis-phen Cu^{II} complex does not show any photoinduced DNA cleavage activity in UV-A and visible light.

(63) Sato, O.; Cui, A.; Matsuda, R.; Tao, J.; Hayami, S. *Acc. Chem. Res.* **2007**, *40*, 361.

(64) Miertus, S.; Scrocco, E.; Tomasi, J. *Chem. Phys.* **1981**, *55*, 117. Miertus, S.; Tomasi, J. *Chem. Phys.* **1982**, *65*, 239. Barone, V.; Cammi, R.; Tomasi, J. *Chem. Phys. Lett.* **1996**, *255*, 327.

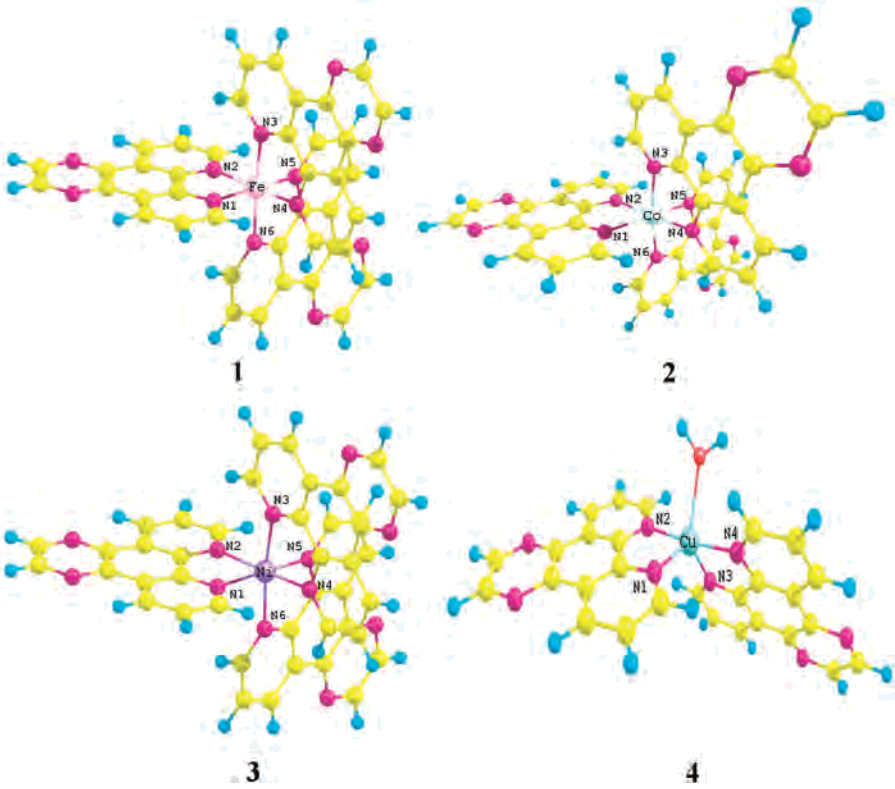

Figure 9. Optimized geometry of complexes **1**−**4**.

Table 3. Selected Geometrical Parameters for the Complexes **1**−**4** with the Experimental Bond Lengths Given in Parentheses for the Structurally Characterized Complex **1**

	Fe^{II} ($t_{2g}^6e_g^0$) (**1**)	Co^{II} ($t_{2g}^5e_g^2$) (**2**)	Ni^{II} ($t_{2g}^6e_g^2$) (**3**)	Cu^{II} (**4**)
M−N1	1.975 (1.980)	2.147	2.113	2.016
M−N2	1.972 (1.973)	2.145	2.113	2.094
M−N3	1.975 (1.970)	2.149	2.112	2.016
M−N4	1.975 (1.964)	2.144	2.112	2.094
M−N5	1.975 (1.986)	2.147	2.115	
M−N6	1.975 (1.980)	2.147	2.112	

from the X-ray structure for Fe^{II} ($t_{2g}^6e_g^0$) (**1**) are found to be close to the values obtained from the optimization at this level. The structures of Co^{II} ($t_{2g}^5e_g^2$) (**2**), Ni^{II} ($t_{2g}^6e_g^2$) (**3**), and Cu^{II} (**4**) are also optimized at this level. The metal−nitrogen distances follow the expected trend based on the electronic configurations. The metal−ligand interactions arising from the e_g orbitals are necessarily M−N antibonding. As the number of electrons in the e_g level increases, the M−N distance increases (Table 3). The single point calculations on the other electronic states are carried out using the optimized geometries of the respective metal complexes. The vertical ionization potential values are calculated for the complexes to support their favorable reaction pathways. To understand the effect of solvent on the photoinduced DNA cleavage activity, we have carried out single point calculations on the gas-phase-optimized geometries using polarizable continuum models (PCM) with parameters corresponding to water ($\mathcal{E} = 78.39$) and nitromethane ($\mathcal{E} = 38.2$). The DMF solvent is not available in the PCM calculations. So, we have used nitromethane ($\mathcal{E} = 38.2$) as a solvent that is almost similar to the DMF ($\mathcal{E} = 38.3$). All the calculations are carried out using the *Gaussian 03* suite of programs.[65]

Table 4. Vertical Ionization Potentials (kcal M^{-1}) of the Complexes **1**−**4** Calculated at the BP86/LANL2DZ Level of Theory

	Fe^{II} (**1**)	Co^{II} (**2**)	Ni^{II} (**3**)	Cu^{II} (**4**)
gas phase	266.26	253.77	337.86	201.06
water	132.72	119.63	147.98	110.47
nitromethane	137.75	123.83	151.83	111.99

The photoredox DNA cleavage is dependent on the ease with which an electron can be released from the metal complex. An estimate of this can be made from the vertical ionization potentials calculated for these complexes. The vertical ionization potential value is calculated for the transformation of the Fe^{II} ($t_{2g}^6e_g^0$) state to the Fe^{III} ($t_{2g}^5e_g^0$) electronic state. For the Co^{II} complex, the ground electronic state is $t_{2g}^5e_g^2$. The other low-lying electronic state, $t_{2g}^6e_g^1$, is 1.13 kcal M^{-1} higher in energy than the ground electronic state. Here, the vertical ionization potential is calculated for the transformation of the Co^{II} ($t_{2g}^6e_g^1$) state to the Co^{III} ($t_{2g}^6e_g^0$) state. Similarly, the vertical ionization potential is calculated for the transformation of the Ni^{II} ($t_{2g}^6e_g^2$) state to the Ni^{III} ($t_{2g}^6e_g^1$) electronic state. For the Cu^{II} complex, it has been reported that the Cu^{II} complex accepts the electron from the reaction medium to form the Cu^{I} complex, which releases the electron to form the Cu^{II} complex. So, the vertical ionization potential is calculated for the transformation of Cu^{I} to the Cu^{II} electronic state. The low vertical ionization potential values for the Co^{II} (253.77 kcal M^{-1}) and Cu^{II} complexes (201.06 kcal M^{-1}) prove the photoredox pathway

(65) Frisch, M. J. et al. *Gaussian 03*, revision C.02; Gaussian, Inc.: Wallingford CT, 2004.

for the DNA cleavage activity (Table 4). Considerably higher values for the respective Fe^{II} (266.26 kcal M^{-1}) and Ni^{II} (337.86 kcal M^{-1}) complexes exclude such a possibility. According to the calculations, the energy required to remove an electron from the 3d transition-metal complexes decreases significantly in water and nitromethane. However, these do not change the trends. The theoretical results show trends similar to those of the experimental data where the metal-based redox potential values are 1.2, 0.4, and 0.09 V for the Fe^{III}/Fe^{II}, Co^{III}/Co^{II}, and Cu^{II}/Cu^{I} couples, respectively.

Conclusions

Metal ions in the complexes of Fe^{II}, Co^{II}, Ni^{II}, Cu^{II}, and Zn^{II} containing the photoactive dpq ligand are found to play an important role in the photoinduced DNA cleavage activity under UV and visible light. The spectral and redox properties of the complexes are of particular importance for the observation of photoinduced DNA cleavage activity in visible light. The diamagnetic Fe^{II} and Zn^{II} complexes show DNA cleavage activity only in UV light, although the Fe^{II} complex has charge-transfer bands with high molar extinction coefficient values. Among the paramagnetic Co^{II}, Ni^{II}, and Cu^{II} complexes, only the Co^{II} and Cu^{II} complexes show DNA cleavage activity in UV and visible light. The Co^{II} and Cu^{II} complexes show metal-based redox potentials that are presumably involved in the photoredox DNA cleavage pathway. The salient observations of this study include DNA cleavage activity at 365 nm involving singlet oxygen for the Fe^{II}, Ni^{II}, Cu^{II}, and Zn^{II} complexes and hydroxyl radical for the Co^{II} species. As the ligands alone are inactive in cleaving SC DNA at 365 nm, involvement of the metal-based charge-transfer bands is proposed in the photoexcitation process. The iron, cobalt, and copper complexes are found to be more active than the nickel and zinc complexes in UV light. Although Fe^{II}, Co^{II}, Ni^{II}, and Cu^{II} complexes show visible spectral bands, only the Co^{II} and Cu^{II} species display visible-light-induced DNA cleavage activity on photoexposure at their visible band. The presence of a visible band is not the only requirement to observe the photocleavage activity in visible light. Although the molar extinction coefficient values of the visible bands of the Fe^{II} complex are significantly high, this complex is cleavage-inactive in visible light, possibly due to the absence of any accessible Fe^{III}/Fe^{II} redox couple. In contrast, the Co^{II} and Cu^{II} complexes are active due to the presence of metal-based redox couples in the range of 0.0−0.4 V vs SCE, facilitating the photoredox pathway. The Co^{II} complex is found to cleave DNA under anaerobic conditions. It is proposed that photoionization of **2** leads to the formation of e_{aq}^{-} that causes DNA cleavage. The results are of significance toward the design and development of 3d-metal based DNA photocleavers under visible light for potential use in PDT. The Co^{II} complex is of particular importance due to its visible-light-induced DNA cleavage activities under hypoxic conditions. The variations in the vertical ionization potentials calculated for the complexes are in tune with the experimental redox potentials and the photoredox DNA cleavage pathway.

Acknowledgment. We thank the Department of Science and Technology (DST), Government of India, and the Council of Scientific and Industrial Research (CSIR), New Delhi, for financial support and the DST for use of the CCD diffractometer facility. We also thank the Alexander von Humboldt Foundation, Germany, for the donation of an electroanalytical system, and the Convener, Bioinformatics Center of our Institute for database search. B.P. and A.K.P. are thankful to the CSIR for fellowships. We acknowledge the Maui High Performance Computing Center (MHPCC) at Hawaii for providing the computational facility.

Supporting Information Available: ORTEP views and unit cell packing diagrams of **1** and **5a** (Figures S1−S4), DNA binding plots (Figures S5−S7), and DNA photocleavage data (Figures S8−S11); cyclic voltammograms (Figure S12); EPR spectrum (Figure S13); variable-temperature magnetic data (Figure S14); mass spectral data (Figures S15−18), electronic spectra (Figure S19); selected crystallographic, bond distance, and bond angle data (Tables S1−S3); full citation of ref 65; tables listing the crystallographic data, atomic coordinates, complete bond distances and angles, anisotropic thermal parameters, and hydrogen atom coordinates for complexes **1** and **5a** (CIF). This material is available free of charge via the Internet at http://pubs.acs.org.

IC701450A